Purge Effect Simulation of Atomic Layer Deposition for High Aspect Ratio Structure

Satoshi Nakamura
Process TCAD Lab
Samsung Device Solutions R&D Japan
Yokohama, Japan
s.nakamura@samsung.com

Hisashi Kotakemori
Process TCAD Lab
Samsung Device Solutions R&D Japan
Yokohama, Japan
h.kotakemori@samsung.com

Kenta Yashima
Process TCAD Lab
Samsung Device Solutions R&D Japan
Yokohama, Japan
k.yashima@samsung.com

Taishi Ikeda
Process TCAD Lab
Samsung Device Solutions R&D Japan
Yokohama, Japan
t.ikeda@samsung.com

Takumi Ohmura
Process TCAD Lab
Samsung Device Solutions R&D Japan
Yokohama, Japan
t.ohmura@samsung.com

Yasuyuki Kayama
Process TCAD Lab
Samsung Device Solutions R&D Japan
Yokohama, Japan
y.kayama@samsung.com

YunTae Lee
CSE Team,
Samsung Electronics
Hwaseong-si, Korea
yuntae11.lee@samsung.com

Gwangsu Yoo
CSE Team,
Samsung Electronics
Hwaseong-si, Korea
gwangsu.yoo@samsung.com

Yukihide Tsuji
CSE Team,
Samsung Electronics
Hwaseong-si, Korea
yuki.tsuji@samsung.com

Shinwook Yi
CSE Team,
Samsung Electronics
Hwaseong-si, Korea
vexgriff.lee@samsung.com

Jaehoon Jeong
CSE Team,
Samsung Electronics
Hwaseong-si, Korea
jh77.jeong@samsung.com

Dae Sin Kim
CSE Team,
Samsung Electronics
Hwaseong-si, Korea
daesin.kim@samsung.com

***Abstract*—We investigated the purge effect in the atomic layer deposition (ALD) process using an in-house voxel-based topography simulator. The simulator incorporates various reaction models, including chemisorption, physisorption, activation at chemisorption and physisorption sites, and purge reactions. These reaction models enable accurate simulation of the actual purge step, which is crucial for controlling film quality and uniformity in ALD. We present simulations of full-cycle ALD processes in trench structures with varying aspect ratios under different purge flux conditions.**

Keywords—ALD, Purge, HARC, Topography, Voxel

I. Introduction

Atomic Layer Deposition (ALD) is a key process for creating uniform thin films in semiconductor manufacturing [1]. In particular, it is widely used for deposition in deep or geometrically complex regions of various semiconductor devices. Applying ALD requires optimizing process conditions, improving production yield, and enhancing throughput in semiconductor fabrication. However, this is challenging because increasing the purge time improves film quality but reduces throughput and increases manufacturing costs. Therefore, it is essential to develop topography simulations for ALD that can capture purge phenomena and support effective process optimization.

A voxel-based topography simulator is a powerful tool for analyzing nanoscale structures in semiconductor processes. One notable feature of this tool is its ability to handle complex surface reactions for realistic process recipes. Building on this strength, we developed an in-house ALD simulator that includes reaction models of chemisorption, physisorption, activation at these adsorption sites, and purge. These reaction models enable the simulation of the purge effect in the ALD, allowing us to evaluate whether undesired material remains due to an insufficient purge step.

Similar reaction models for ALD have also been implemented in previous voxel-based topography simulators [6-10]. These simulators adopt a model in which each voxel corresponds to a single simulation-solid-particle. While this approach naturally accommodates reaction models that depend on the bonding states of neighboring solid particles, such as physisorption and purge reaction, it requires an extremely large number of voxels to represent atomic layer structures in actual devices. In contrast, Ref. [5] adopts a model in which a single voxel represents multiple simulation-solid-particles, significantly reducing the number of required voxels. However, this approach has lacked a mechanism to handle reactions that depend on the bonding states of neighboring solid particles; therefore, the purge effect has been ignored in previous tools [2-10].

To address this limitation, we propose a novel scheme that enables the simulation of bonding-state-dependent reactions even when using a single voxel for multiple simulation-solid-particles. This scheme allows for more efficient ALD purge effect simulations, reducing computation time and memory usage compared to previous tools. Finally, we present full-cycle ALD simulations in trench structures with varying aspect ratios under different purge flux conditions.

II. Modeling

The simulation flow of our in-house simulator consists of (1) Create voxel data (2) Monte Carlo (MC) particle transport, (3) reaction judgment between an MC particle and solid particles in the voxel where the MC particle arrives, and (4) voxel data updates corresponding to reaction execution. These phases are repeated for each MC particle.

In phase (1), we introduce voxel variables $n_{\mathrm{R}}(i,m)$ and $n_{\mathrm{I}}(i,m)$, which correspond to the volume fraction of the initial structure. Here, i denotes the cell ID and m denotes material ID. We assume that each voxel contains both reactive and non-reactive inner spaces, with multiple simulation-solid-particles present in both spaces, as shown in Fig. 1(a) and (b). $n_{\mathrm{R}}(i,m)$ and $n_{\mathrm{I}}(i,m)$ denote the number of particles of material m in the reactive and inner spaces of voxel i, respectively. The maximum number of $n_{\mathrm{R}}(i,m)$ is denoted as N_{smax}, the maximum number of $n_{\mathrm{I}}(i,m)$ is denoted as N_{imax}, and the maximum total number of solid particles in a voxel is denoted as $N_{\mathrm{max}} = N_{\mathrm{smax}} + N_{\mathrm{imax}}$. Therefore, the total number of particles in the voxel is $n(i) = \sum_m\{n_{\mathrm{R}}(i,m) + n_{\mathrm{I}}(i,m)\}$ and the volume fraction of the voxel is given by $n(i)/N_{\mathrm{max}} = \sum_m\{n_{\mathrm{R}}(i,m) + n_{\mathrm{I}}(i,m)\}/(N_{\mathrm{smax}} + N_{\mathrm{imax}})$. This approach effectively reduces the number of voxels, even when one simulation-solid-particle corresponds to one real solid particle.

Various reactions are modeled by introducing rules that determine how voxel variables change when an MC particle reaches the voxel. in phase (3), the reaction is determined based on the pair of the MC particle and a selected solid particle in the reactive space of the voxel. In phase (4), voxel structure is updated according to the reaction determined in phase (3). A detailed voxel update for a normal deposition reaction, represented by $A\langle g\rangle + B\langle s\rangle = C\langle s\rangle + B\langle b\rangle$, is as follows. Here, $A\langle g\rangle$ is the gas MC particle calculated in phase (2), $B\langle s\rangle/B\langle b\rangle$ is the target solid particle, selected in phase (3), $C\langle s\rangle$ is the deposited solid particle. If the number of solid particles n in the voxel is smaller than N_{smax}, the number of particles in the reactive space n_{R} for material C is incremented. In the case where $N_{\mathrm{max}} > n \geq N_{\mathrm{smax}}$ and n_{R} for C is N_{smax}, the number of particles in the inner space n_{I} for C is incremented (Fig. 1 (e)). This is the fundamental principle underlying the calculation in our in-house simulator.

We model ALD reactions by introducing additional voxel variables representing various types of reactive sites, such as physisorption and chemisorption. The reactive sites originate from bonding states: chemisorption refers to adsorption due to electron transfer and forms stronger bonds, whereas physisorption is governed by van der Waals forces and forms weaker bonds. Therefore, if sufficient purge gas is supplied, physisorbed material will desorb, while chemisorbed material will remain adsorbed. Furthermore, while chemisorption exhibits self-limitation and can react only at normal reactive sites, physisorption can react at sites such as normal reactive sites, chemisorbed site, and physisorbed site.

Here, we define four voxel variables to model this behavior: $n_{\mathrm{C}}(i,m)$ represents the number of chemisorption sites, $n_{\mathrm{SP}}(i,m)$ the number of single physisorption sites, $n_{\mathrm{DP}}(i,m)$ the number of double physisorption sites, and $n_{\mathrm{TP}}(i,m)$ the number of triple physisorption sites. These voxel variables enable us to characterize these bonding characteristics at the voxel level. Using these variables allows us to model the effects of purge reactions, where purging acts like a sputtering reaction that affects only particles adsorbed via physisorption. Therefore, we need to identify the bonding states of the target particles during the ALD process to simulate the purge effect (Fig. 1(c)).

A detailed voxel update for the chemisorption and physisorption processes is described below (Fig. 1(f)). The chemisorption reaction is executed only when $n_{\mathrm{N}}(i) \equiv \sum_m\{n_{\mathrm{R}}(i,m) - n_{\mathrm{C}}(i,m) - n_{\mathrm{SP}}(i,m) - n_{\mathrm{DP}}(i,m) - n_{\mathrm{TP}}(i,m)\} > 0$. This voxel update is similar to a typical deposition reaction; however, both $n_{\mathrm{R}}(i,m)$ and $n_{\mathrm{C}}(i,m)$ are incremented upon deposition. Here, $n_{\mathrm{N}}(i)$ represents the number of normal sites in voxel i. Physisorption occurs under three conditions: if $n_{\mathrm{C}}(i,m) > 0$, if $n_{\mathrm{SP}}(i,m) > 0$, or if $n_{\mathrm{DP}}(i,m) > 0$. The voxel update for physisorption is also similar to a normal deposition reaction. However, both $n_{\mathrm{R}}(i,m)$ and $n_{SP}(i,m)$ are incremented if $n_{\mathrm{C}}(i,m) > 0$. In addition, $n_{\mathrm{DP}}(i,m)$ and $n_{\mathrm{TP}}(i,m)$ are incremented if $n_{\mathrm{SP}}(i,m) > 0$ and $n_{\mathrm{DP}}(i,m) > 0$, respectively. These new voxel variables allow us to determine whether a purge reaction occurs.

III. Purge Effect Simulation

We demonstrate a simulation of the purge effect in ALD processes to create a metal thin film on silicon using the in-house ALD simulator. The ALD cycle follows the sequence illustrated in Fig. 2(a). The simulation performs 10 cycles, each comprising an adsorption step with gas A, a purge step with gas N, and an activation step with gas B. The duration times of gases A, N, and B are T_{A} =10 sec, T_{N}=40 sec, and T_{B} =20 sec, respectively. In Step 1, gas A reacts with the silicon surface through physisorption and chemisorption. Gas N reacts with physisorbed species via purge reactions, and gas B reacts at both physisorption and chemisorption sites during activation step. If the purge effect is insufficient, physisorption sites remain after Step 2. In Step 3, chemisorption sites contribute to metal formation, while non-purged physisorption sites result in undesired material growth (Fig. 2(b) and 2(c)). In our simulation, Step 4 is ignored, because it has negligible impact on structural evolution. The effectiveness of the purge process depends on the purge flux, purge time, and target structure.

The following reaction set is employed in the simulation:

No	Reaction Type	Gas	Surface material	Product	Probability
(1)	Chemisorption	A	Si	C (c)	0.3
(2)	Chemisorption	A	M	C (c)	0.3
(3)	Chemisorption	A	D	C (c)	0.3
(4)	Physisorption	A	C (c)	C (p)	0.001
(5)	Physisorption	A	C (p)	C (p)	0.001
(6)	Purge	N	C (p)	--	1.0
(7)	Activation	B	C (c)	M	0.9
(8)	Activation	B	C (p)	D	0.1

where Si denotes silicon, M denotes the forming metal layer. Material C (c) and C (p) represent the intermediate species via chemisorption and physisorption, respectively. Material D represents the non-purged material. Reactions (1)–(5) describe the adsorption step, reaction (6) describes the purge step, and reactions (7)–(8) correspond to the activation step. As summarized above, these reactions dictate the progression of the simulated ALD process.

Figure 3 shows the simulation results using the model explained in Section II. The initial structure is a rectangular trench structure etched into a silicon wafer, as shown in Figs. 3(a) and 3(b). A metal layer is deposited with uniform coverage on the silicon base with a purge flux of 10^{-3}[mol/m^2/s], as shown in Figs. 3(c) and 3(d). Figure 3(e) displays the distribution of the non-purged material, excluding silicon and metal. Furthermore, we demonstrate the purge

effect by varying the purge flux in Figs. 3(f) and 3(g), where the distributions of non-purged material at purge fluxes of 10^{-5} and 10^{-10} [mol/m^2/s], respectively. The non-purged material spreads over the silicon surface at a low purge flux, whereas it remains only in the bottom of the trenches at a high purge flux.

IV. ALD for High Aspect Ratio Structure

We investigate an ALD process applicable to high aspect ratio structures. Initial structures are prepared with aspect ratio (AR) of 5, 10, 20, and 50, corresponding to diameters of 40 nm and heights of 0.2 µm, 0.4 µm, 0.8 µm, and 2 µm, respectively (Figs. 4(a), (b), and (d)). The ALD process utilizes the gas sequence and reaction set as described in Section III. Adsorption durations T_A are varied depending on the aspect ratio: T_A=1 sec (AR=5), 2 sec (AR=10), 20 sec (AR=20), and 500 sec (AR=50). The activation duration (T_B) is fixed at twice the value of T_A. All fluxes are maintained at 10^{-3}[mol/m^2/s], and probabilities for reactions (1)-(3) and (6)-(8) are set to 0.5, and probabilities for reactions (4) and (5) are set to 10^{-5} for all AR values. Figure 4(c) shows a final structure achieved after 10 ALD cycles for AR=5 without physisorption. Furthermore, we analyze the thickness of the deposited metal and residual non-purged material versus position z for AR=50 case. Therefore, longer purge times approximate the ideal ALD, even including physisorption. Conversely, short purge times result in the presence of residual non-purged materials, consistent with the results in Section III (Figs. 4(e) and (f)).

Lastly, we evaluate the thickness and deposition volume of non-purged material across various aspect ratio and purge durations. We assume 5 cycle ALD with 10^{-4} of probabilities for reactions (4) and (5) to enhance clarity of trends. As shown in Figs. 5 (a)–(e), while sufficiently long purge times achieve ideal ALD process, the necessary purge duration depends on aspect ratio of the structure.

V. Conclusion

We developed in-house voxel-based topography simulator of ALD process. We introduced a novel method utilizing voxel variables to determine the bonding states of solid particles. This method enables the simulation of the purge effect even with multi-particle voxels. Importantly, it maintains the advantages in computational time and memory usage relative to models with single-particle-per-voxel approaches. We also demonstrated purge effect simulations with various purge fluxes for various aspect ratio structures. Our findings show good agreement between simulated and expected material distributions, demonstrating dependencies on both purge time and aspect ratio. Therefore, we expect that the simulator will be valuable in optimizing process parameters during actual process development.

References

[1] Steven M. George, Chem. Rev. **110**, 111-131 (2010).

[2] N. Kuboi, Jpn. J. Appl. Phys. **63**, 080801 (2024).

[3] R. J. Hoekstra and M. J. Kushner, J. Vac. Sci. Technol. B, **16**, 2102 (1998).

[4] Chad M. Huard, PhD Thesis (2018).

[5] P. Regli, G. Bozza, US10599789B2 (2020).

[6] P. Moroz, and D. J. Moroz, J. Phys.: Conf. Ser. **550**, 012030 (2014).

[7] X. Meng, Y. C. Byun, H. S. Kim, J. S. Lee, A. T. Lucero, L. Cheng, and J. Kim, Materials, **9**(12), 1007 (2016).

[8] K. Denpoh, P. Moroz, T. Kato, and M. Matsukuma, Jpn J. Appl. Phys. **59**, SHHB02 (2020).

[9] Qu, Y. Sakiyama, P. Agarwal and M. J. Kushner, J. Vac. Sci. Technol. A **39**, 052403 (2021).

[10] N. Kuboi, H. Matsugai, T. Tatsumi, S. Kobayashi, Y. Hagimoto, and H. Iwamoto, Jpn. J. Appl. Phys. **62**, SI1006 (2023).

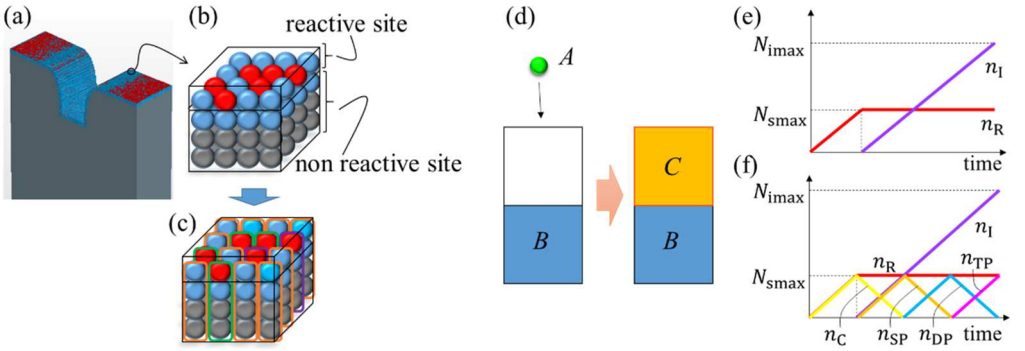

Fig. 1. (a) Example of voxel structure (b) A voxel in our simulator (c) A voxel for ALD model to determine the bond states. (d) Example of a voxel structure update. Particles of gas A arrive at the blue voxel filled with material B, and material C is deposited in the orange voxel. (e) Voxel variable updates during the normal deposition reaction as shown in Fig. 1(d). The transitions of n_R and n_I for material C in the orange voxel is shown. (f) Voxel variable updates during the chemisorption/physisorption reactions as shown in Fig. 1(d). The transitions of n_R, n_I, n_C, n_{SP}, n_{DP}, and n_{TP} for material C in the orange voxel is shown.

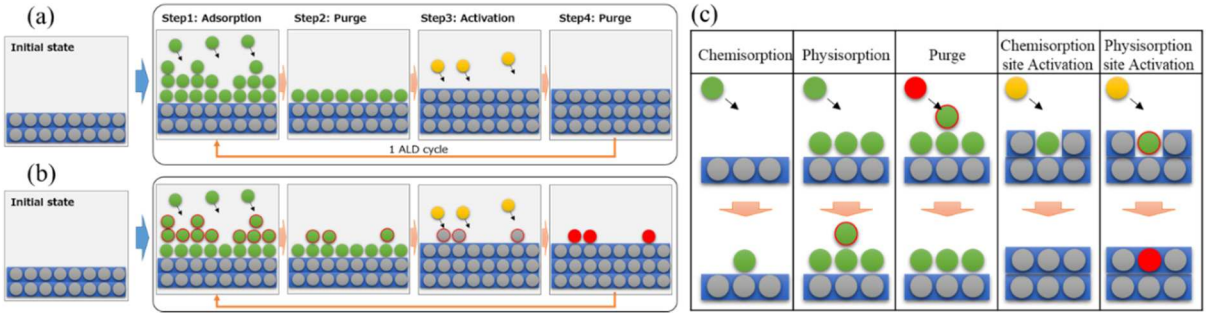

Fig. 2. (a) ALD cycle for ideal process (b) ALD cycle for insufficient purge process (c) ALD reaction models in our simulation

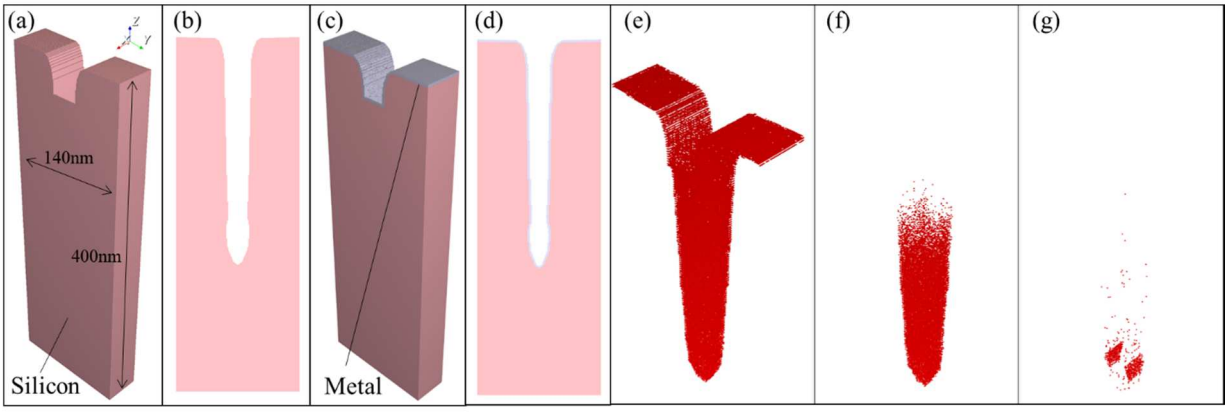

Fig. 3. Purge effect simulation (a) Initial structure 3D (b) Initial structure 2D plane cut (c) Result structure 3D (d) Result structure 2D plane cut. (e) Non-purged material distribution in purge effect demonstration for Purge flux = 10^{-10} mol/m^2/s (f) Purge flux is 10^{-5} mol/m^2/s (g) Purge flux is 10^{-3} mol/m^2/s.

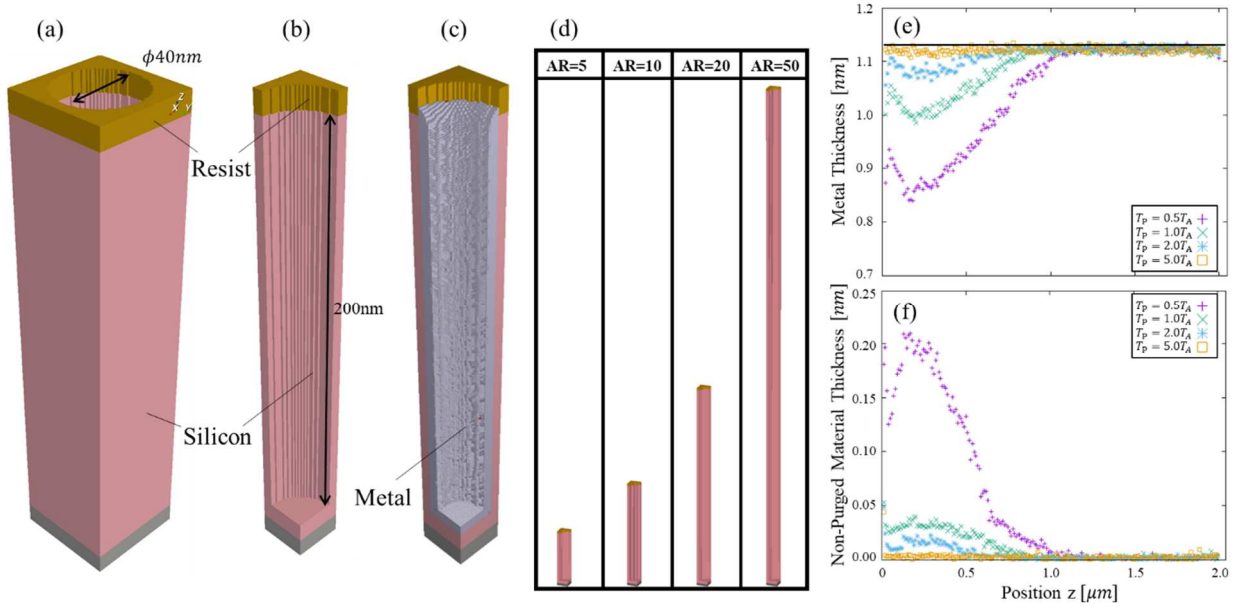

Fig. 4. ALD for high aspect ratio structure (a) Initial structure of the AR=5 trench (b) Initial structure of the AR=5 trench: 1/4 cut (c) Final structure of the AR=5 trench: 1/4 cut (d) Initial structures for AR= 5, 10, 20, and 50 with heights of 200nm, 400nm, 800nm, and 2000nm, respectively. (e) Metal thickness of 5 cycle ALD for AR=50 with various purge time. We define z=0 at the top surface of deposited metal on the bottom surface of the trenches. (f) Residual non-purged material thickness of 5 cycle ALD for AR=50 with various purge time.

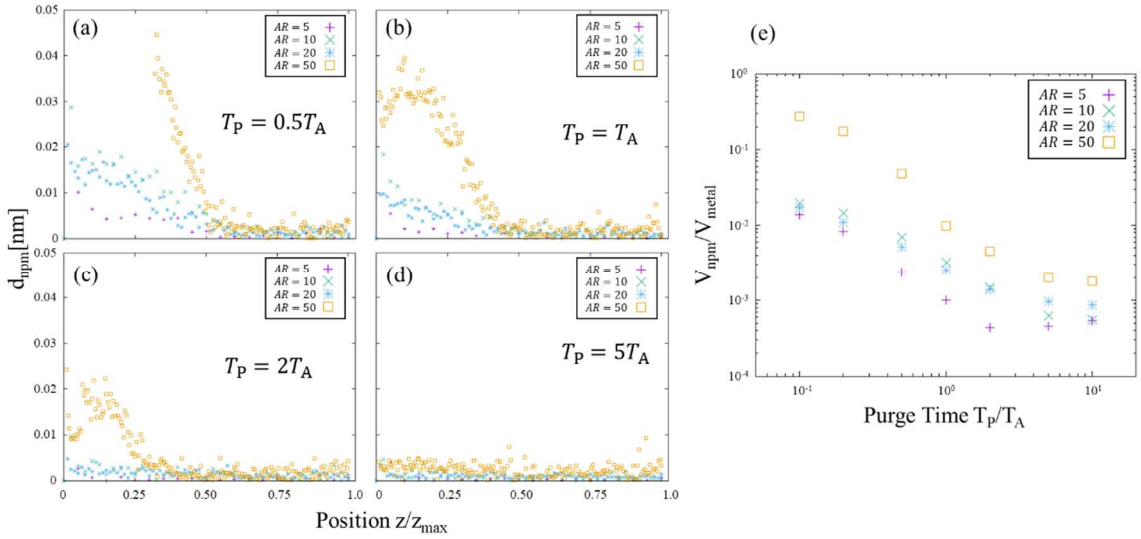

Fig. 5. ALD for various AR (a) Non-purged material thickness d_{npm} vs position z/z_{max} for AR=5, 10, 20, and 50 with $T_{\mathrm{P}} = 0.5T_{\mathrm{A}}$. (b) $T_{\mathrm{P}} = T_{\mathrm{A}}$. (c) $T_{\mathrm{P}} = 2T_{\mathrm{A}}$. (d) $T_{\mathrm{P}} = 5T_{\mathrm{A}}$. (e) Ratio of non-purged material volume V_{npm} and depositted metal volume V_{metal}vs purge time $T_{\mathrm{p}}/T_{\mathrm{a}}$ for AR=5, 10, 20, and 50.